168

SATELLITE & MESOMETEOROLOGY
RESEARCH PROJECT

Department of the Geophysical Sciences
The University of Chicago

STUDY OF A SPLITTING ANVIL OVER IOWA ON MAY 15, 1977, USING 3-MINUTE SMS AND LEAR JET PICTURES

Duane J. Stiegler

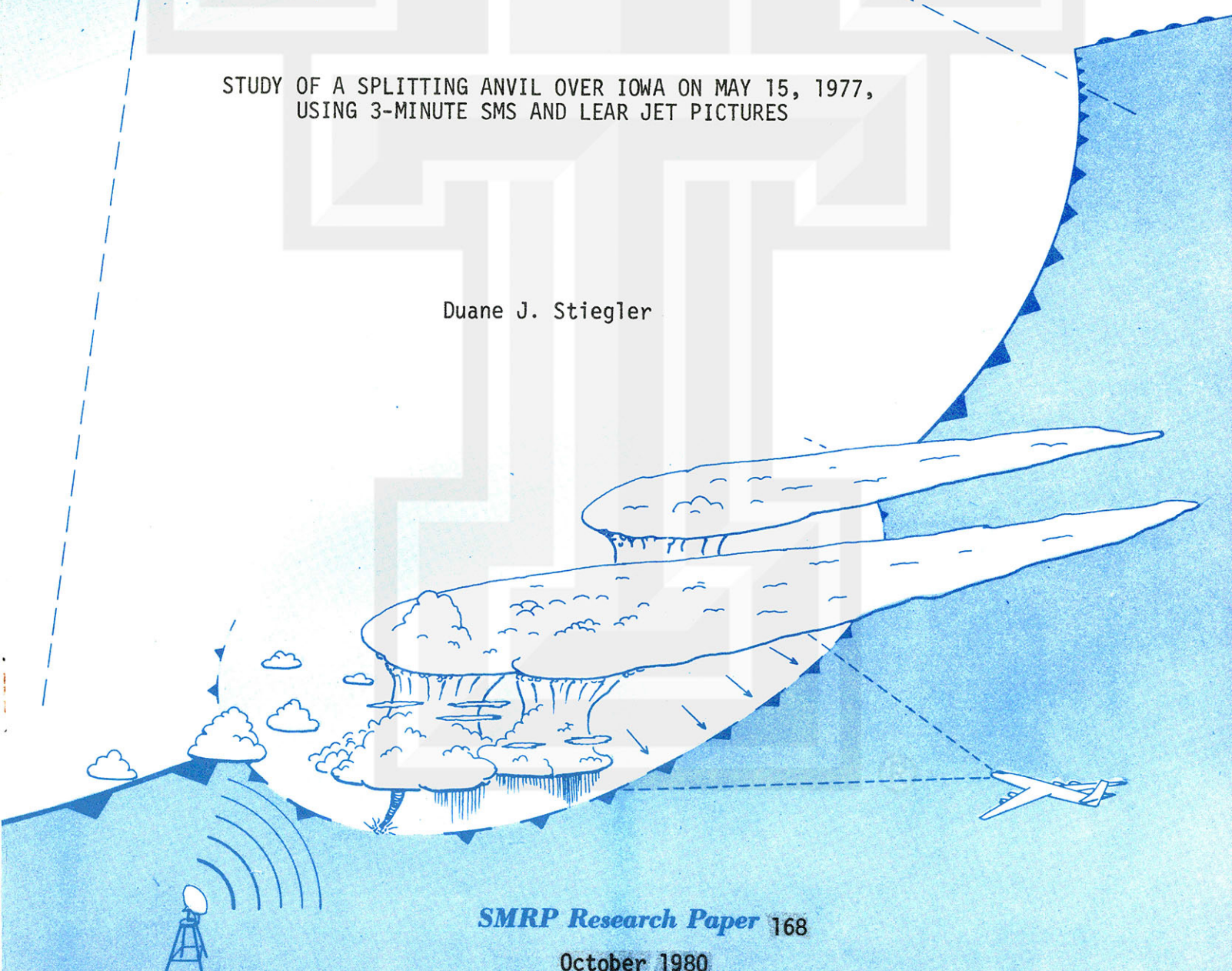

SMRP Research Paper 168

October 1980

STUDY OF A SPLITTING ANVIL OVER IOWA ON MAY 15, 1977, USING 3-MINUTE SMS AND LEAR JET PICTURES

Duane J. Stiegler
Department of the Geophysical Sciences
The University of Chicago

SMRP Research Paper No. 168
October 1980

Study Of A Splitting Anvil Over Iowa On May 15, 1977, Using 3-Minute SMS And Lear Jet Pictures

by

Duane J. Stiegler

ABSTRACT

A dramatic case of anvil splitting near Des Moines, Iowa was studied through the use of 3-minute SMS and Lear Jet photographs. The storm was situated in an area of vigorous upper divergence and only slight low-level convergence. The split and subsequent decay is related to a strong horizontal shear associated with a passing mesoscale wave. Many of such waves were evident in the analysis and showed a marked effect on cloud formation and dissipation. The waves were characterized by two north-south bands: a cloud (bright) band immediately followed by a cloud-free (dark) band. The 14 km band separation gives a measure of the half-wavelength of the mesoscale wave.

6,480 cloud-motion vectors were obtained using SMS pictures taken at 3 minute intervals. Most of the tracked low-level clouds are 0.7 to 2.0 mile cumulus turrets, which are likely to move with sub-cloud winds. Comparison of low-level winds with cloud-motion vectors revealed that these vectors do not always coincide.

The cloud heights were determined using the geometry of the sun, cloud and shadow relationship. By way of this method, clouds were accurately grouped by type and height, providing a high degree of confidence with which to interpret their motions.

1. INTRODUCTION

Determination of the representativeness of satellite-derived cloud motions in relation to actual winds has been the main focus of most studies, with the eventual objective of implementing the cloud-deduced winds into synoptic analyses. With the arrival of improved satellite resolution, the ability to observe and quantify the small, short-lived motions associated with mesoscale phenomena has also improved. Fujita, Pearl and Shenk (1975) pointed out that the tracked motions of small overland cumuli could lead to mappings of detailed flow patterns otherwise unobtainable from conventional surface observations. Present and future study of these motions is not only important for the proper interpretation of mesoscale features, but may also serve to improve the forecasting, detection and warning of their severe weather events.

Tecson, Umenhofer and Fujita (1977) showed that mesoscale patterns could be observed from the cloud-motion vectors obtained from 5-minute SMS/GOES visible image sequences. However, few of the low-level overland cumuli were trackable due to their rapid changes and short life. Fujita (1970) reported that 2 - 3 mile convective clouds have a mean life of only 23 minutes. Yet, by virtue of its small degree of interaction with ambient winds, the even smaller cumulus turret (0.3 - 2.0 mile) has been shown to be the best target from which to infer subcloud winds (Fujita et al., 1975). It was thereby concluded that if one is to investigate low-level wind

over land, 3-minute interval imagery will be needed.

As of Spring 1977, 3-minute interval SMS/GOES visible imagery has become available on a research experiment basis. One of the first days of such rapid scan coverage was requested by Fujita for May 15, 1977 in anticipation of the occurrence of thunderstorm activity in the midwestern U.S. To supplement the satellite data, photographic data was simultaneously collected from a Lear Jet manned by University of Chicago staff members, Forbes, Umenhofer, and the author, as part of the U. of C./NASA Cloud Truth Experiment. The purpose of this case study is to investigate the mesoscale disturbances illustrated by cloud motions obtained from 3-minute SMS imagery, while providing comment on the usefulness of the imagery itself.

2. SYNOPTIC AND MESOSCALE ANALYSIS

Cloud-motion analyses based on the 3-minute pictures were performed for the period 1930 to 2100 GMT over an area covering the state of Iowa. Upper-air and surface charts before and after the cloud-tracking periods are presented in Figure 1.

The synoptic situation is characterized by a strong upper short wave entering the central U.S. as it propagates around a stationary cut-off low over the Pacific Ocean off the coast of Washington. A surface low is centered over the western edge of the Nebraska-South Dakota border. As the wave progresses northeastward, a strong southeasterly jet, evident in both 200 MB and 500 MB charts, develops along its leading edge. This jet coincides with a band of moisture at 500 mb in what would otherwise be considered a dry situation at these levels. The large velocity and directional windshift across the state of Iowa should be noted.

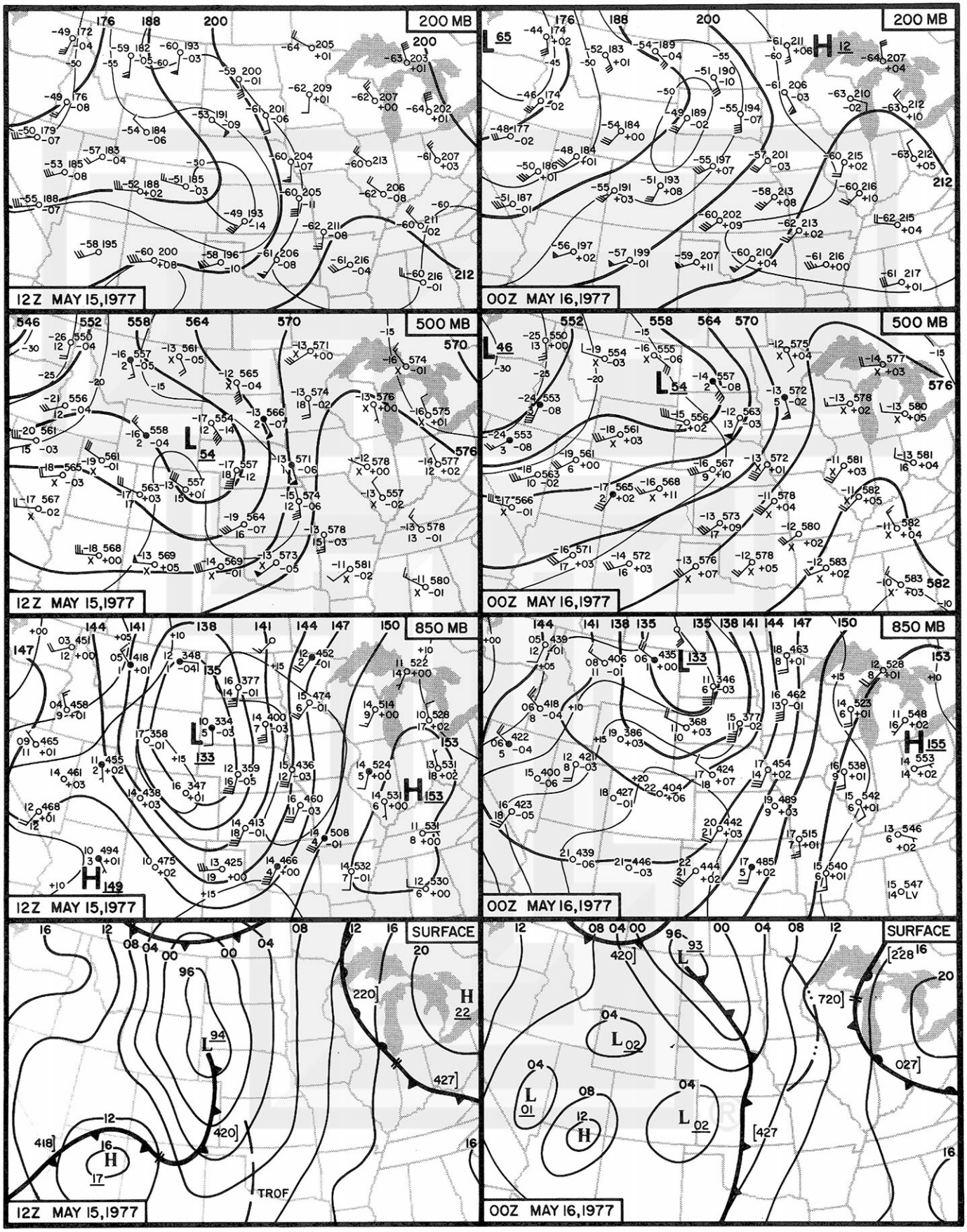

Figure 1. 200 MB, 500 MB, 850 MB, and surface charts for 1200 GMT, May 15, 1977 and 0000 GMT, May 16, 1977.

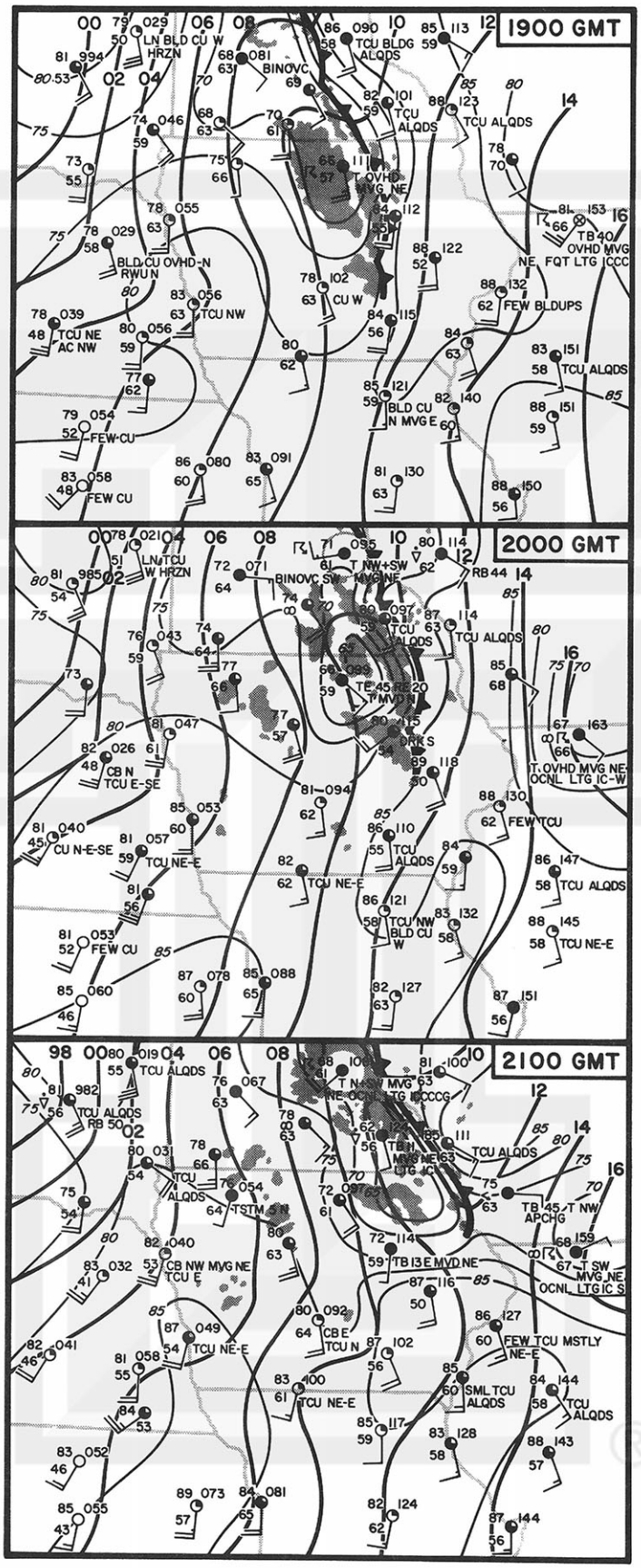

Figure 2. Mesoanalyses based on local area surface observations with superimposed radar echos for 1900, 2000, and 2100 GMT, May 15, 1977. Analyses cover the periods of cloud-motion analyses. Marseilles (MMO) radar is unavailable.

The deepening wave is best shown in the large height falls of the 12 Z analyses. With the rapid northeastward progression of the wave, the height rises to the rear of the wave are already exceeding the height falls ahead at 00 Z. This indicates the weakening state of the wave and results in the reformation of the surface low further to the north over the U.S. - Canada border. Prefrontal thunderstorm activities occurred along an instability line which passed through southern Minnesota and northern Iowa, though sooner and to a lesser degree than had been previously expected.

Figure 2 shows three mesoanalyses based on hourly surface observations for 1900, 2000 and 2100 GMT. Echos from NWS radars at Minneapolis, Minn. (MSP), Des Moines, Ia (DSM) and St. Louis, Mo. (STL) are superimposed. The charts depict the thunderstorm development along the instability line for the period of cloud-motion tracking. A second line of cells formed on a north-south stationary front to the east along the west shore of Lake Michigan. These cells, however, do not enter into the area of analysis.

The winds depict an overall confluence in the southerly surface flow of the cyclonic circulation centered to the west. As is expected, the winds generally increase to the west where the pressure gradient is tight. Through the period, isobar spacing becomes disproportionate due to the passage of numerous mesoscale waves shown later. In section 4, particular attention is focused on a small cell shown by the radar echo which moves from southeast to east of Des Moines between 2000 and 2100 GMT.

3. ANALYSIS OF SATELLITE VISIBLE IMAGES

3.1 CLOUD HEIGHT

The major contributing factor to the problem of assimilating cloud motions to ambient windflow has been the uncertainty of cloud height (Hubert and Whitney, 1971). Several methods of obtaining cloud height from satellite imagery have been used in the past. Hubert and Whitney proposed the use of the "Level of Best Fit" (LBF), which assumes the cloud height to be the level of the minimum vectorial difference between the cloud motion and winds obtained from a nearby sounding. Most subsequent methods assume the cloud height derived from infra-red and visible imagery through calculations of the clouds radiant parameters. However the intense vertical motions of mesoscale features such as thunderstorms are known to significantly modify the temperature structures of their environment, especially at the cloud top (see Fujita, 1974). This implies that for mesoscale features, heights based on cloud top temperature alone may be inaccurate. An alternative to this problem is to calculate the cloud top height through geometric means.

Cloud heights in this paper were obtained by using the geometry of the sun, cloud, and shadow relationship (see Appendix). Fujita (1970) postulated that without an extreme resolution (0.1 or 0.2 mile) such a method would not be usable. It was found, however, that some shadow features on the 0.5 mile resolution images could be identified with their cloud tag counterpart. Also, by greatly enlarging the images, measurement of the displacement between the corresponding points was possible.

Cloud heights were obtained from two SMS images, 1939 and 2048 GMT, corresponding to the beginning and end of the cloud-tracking period. A lack of any discernable difference in the resulting data sets warranted

their combination into the single data set shown in Table 1.

Table 1. Cloud heights as derived from the geometry of the sun, cloud and shadow relationship (see Appendix).

Category	Cloud Type	Pop.	Height Range (MSL)	Mean Height
High Clouds	Jet Cirrus	4	9.3 - 10.6 km	10.0 km
	Anvil Cirrus and Cirrus Bands normal to flow	9	6.3 - 8.2	7.2
Low and Middle Clouds	Large Towering Cumuli	11	3.6 - 5.3	4.4
	Small Cumuli (0.7 - 2.0 mi)	28	1.6 - 3.5	2.6

Cloud heights are separated into two categories: "High Clouds" and "Low and Middle Clouds" for tracking and presentation convenience. The height data are further broken down into four naturally occurring groups by cloud type. The population, range and mean is given for each.

The results in Table 1 compare well with a special rawinsonde sounding taken at Omaha at 1800 GMT. The sounding, shown in Figure 3, was taken 1.5 hours prior to the cloud tracking period and at the upwind edge of the analysis area, making it reasonably representative of the analysis conditions. The 10 km mean height of the jet associated cirrus corresponds exactly to the maximum wind level of the sounding. The anvil cirrus heights coincide with moisture band between 400 and 450 MB, with the high end of the range being limited by a pronounced inversion at 350 MB. All of the low to middle cloud heights are above the 1.5 km lifted condensation level and, being of vertically developed cumuli, extend in range to near the anvil cirrus height.

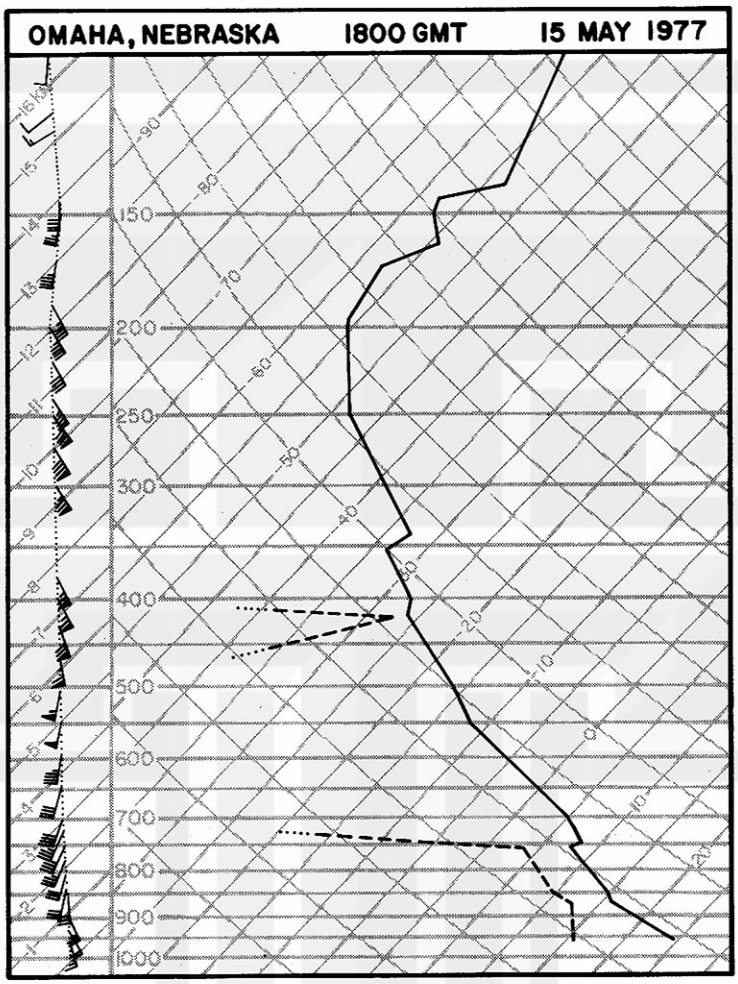

Figure 3. Special sounding taken at 1800 GMT, May 15, 1977 from Omaha, Nebraska. Winds are given in knots on the left as a function of the height in kilometers. The LCL is at 1.5 km or about 840 MB.

Due to the 0.5 mile resolution selected, the sample of cloud heights shown here is small. As was suggested by Fujita, if better results are to be attained, higher resolution imagery will be needed. Such imagery would also enhance the results obtained from stereo satellite observations as have recently been studied.

3.2 CLOUD MOTION

Cloud-motion vectors were computed using the MEteorologist - TRAcking - COMputer (METRACOM) Interactive System developed at the University of Chicago. Details of this system are reported by Chang, Tecson and Fujita (1973). Tracking rules are described by Tecson et al. (1977). Manual tracking was performed on four movie loops, each made from 3 consecutive SMS images covering a 6 minute period. The computed cloud motions were plotted on the initial frame of each loop and are presented in Figures 4, 5, 6 and 7. The periods were selected on the basis of 3-minute interval picture continuity.

As this paper is concerned with the motions associated with mesoscale processes, all trackable cloud motions were superimposed upon the pictures. This allows the observer a freedom of interpretation as to the validity of individual cloud motions in relation to each other, the flow field and the cloud appearance.

The short, 6-minute tracking periods allowed a large number of clouds to be tracked. Table 2 shows the total vectors fitting the two cloud height categories for each of the four movie loops. In all, 6,480 cloud-motion vectors were obtained. Fewer low-level clouds were tracked on the last two loops than on the first two, due to: 1. the increased cirrus coverage, and 2. the lower sun angle, making cloud identification and tracking more difficult. For the sake of clarity, some vectors in congested areas are omitted from the figures presented.

The cloud motion fields show little sign of localized convergence at the low cloud levels, while strong divergence is demonstrated throughout the high cloud levels. A marked velocity increase at all cloud levels is

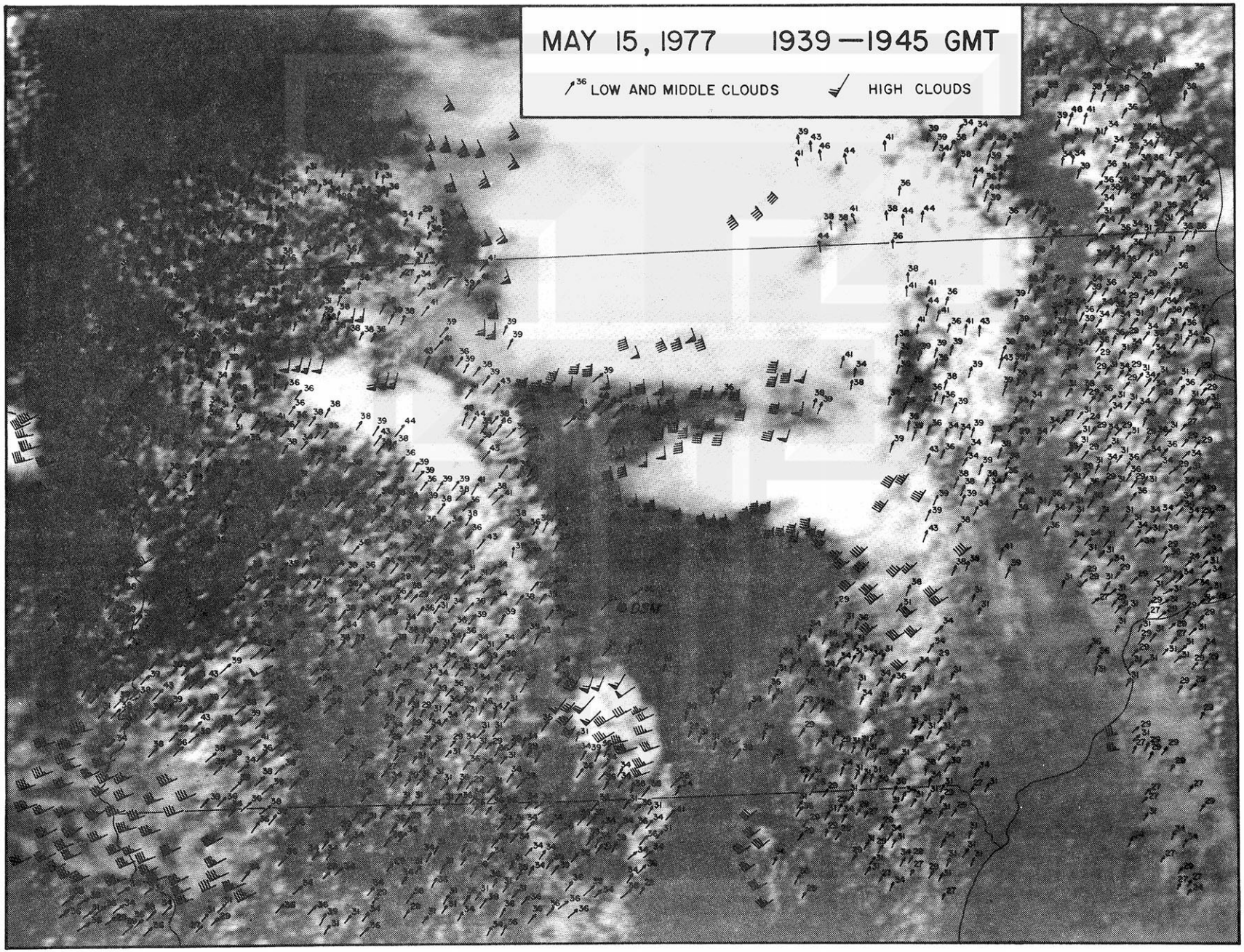

Figure 4. Cloud motion vectors computed from 3, 3-minute SMS pictures at 1939 to 1945 GMT, May 15, 1977 over Iowa. Time of picture is 1939 GMT. Speeds are in knots.

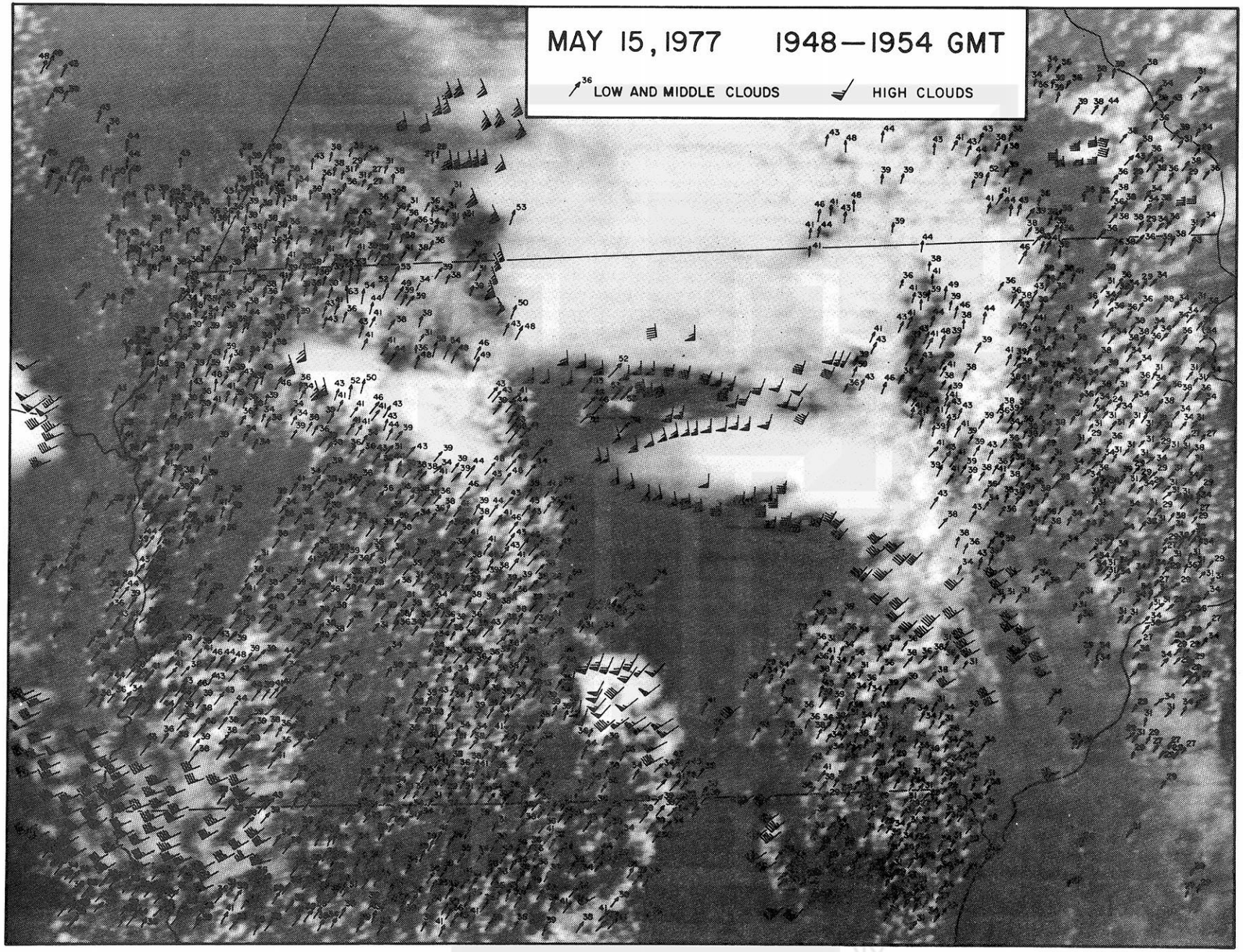

Figure 5. Cloud motion vectors computed from 3, 3-minute SMS pictures at 1948 to 1954 GMT, May 15, 1977 over Iowa. Time of picture is 1948 GMT. Speeds are in knots.

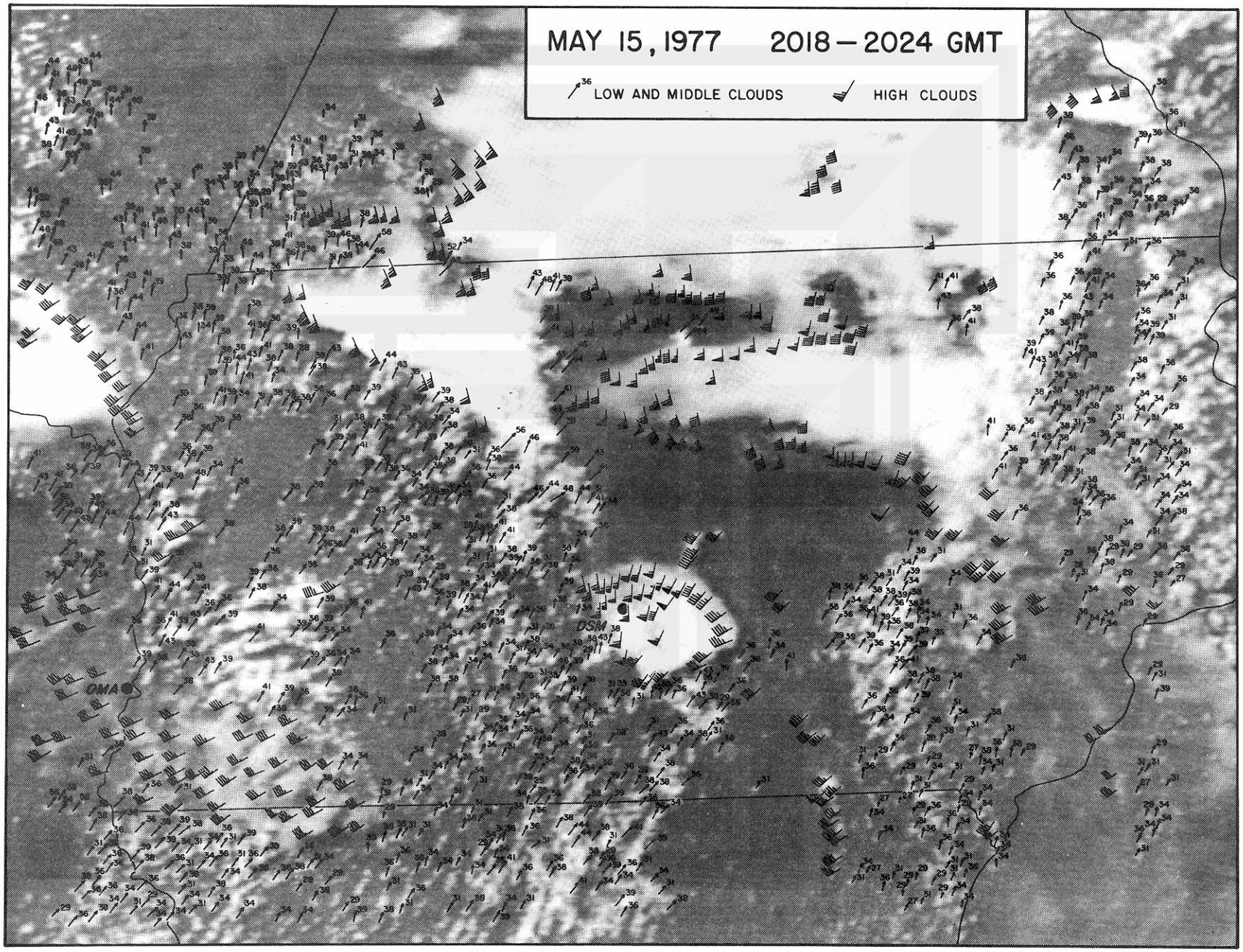

Figure 6. Cloud motion vectors computed from 3, 3-minute SMS pictures at 2018 to 2024 GMT, May 15, 1977 over Iowa. Time of picture is 2018 GMT. Speeds are in knots.

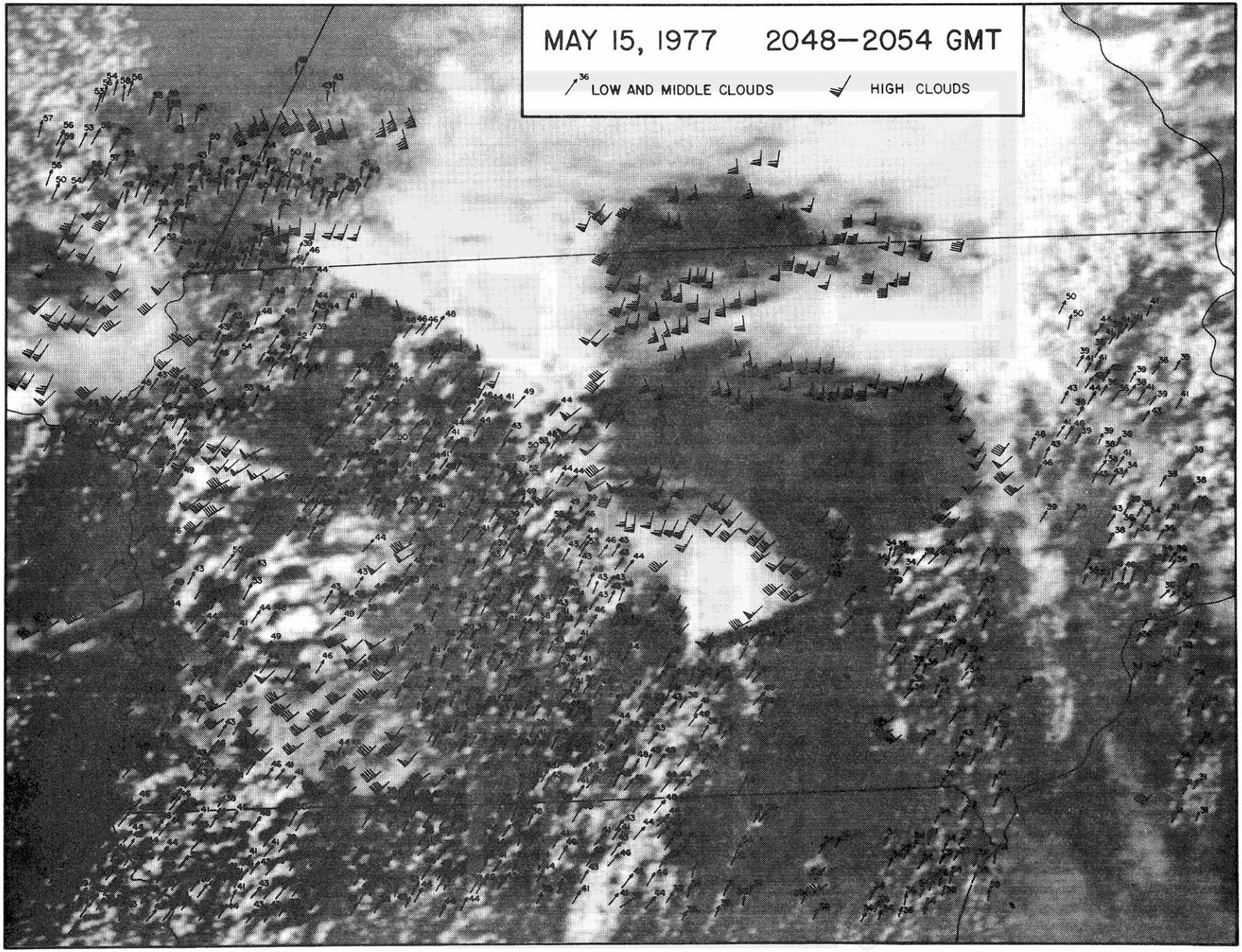

Figure 7. Cloud motion vectors computed from 3, 3-minute SMS pictures at 2048 to 2054 GMT, May 15, 1977 over Iowa. Time of picture is 2048 GMT. Speeds are in knots.

Table 2. The total numbers of high and middle to low cloud vectors for each of the four movie loops on which tracking was performed.

Movie Loop Period (GMT)	High Cloud Vectors	Low & Middle Cloud Vectors	Total Vectors
1939 - 1945	236	1,536	1,772
1948 - 1954	282	1,733	2,015
2018 - 2024	363	1,036	1,399
2048 - 2054	372	922	1,294
Total Vectors	1,253	5,227	6,480

evident through the time sequence illustrated by Figures 4 through 7. The variation of cloud motions within the flow feilds can be explained by a combination of three factors:

1. tracked cloud elements were of varying height and size
2. error was induced from inaccurate tracking
3. cloud motions revealed actual cloud interaction and/or other mesoscale flow characteristics.

Unfortunately, it is not possible to easily distinguish what degree of influence each of these factors contributes to a given variation in the flow field. However, these analyses do give a detailed, quantitative measure of mesoscale flow patterns that cannot be obtained from present operational satellite and rawinsonde observations.

The majority of the tracked low clouds are small cumuli with a diameter range of 0.7 - 2.0 miles. They conform in size to a 0.3 - 2.0 mile cumulus turret classification, described by Fujita et al. (1975) as best targets from which to infer winds within subcloud layers. In this case, a windshift is evident at 1.5 km on the Omaha sounding in Figure 3, indicating a horizontal shear in the vertical. This level is coincidentally

the height of the lifted condensation level. The cloud motions deviate to the right of the winds below the windshift by as much as 45°, and about 35° on the average. Since these motions correspond best with winds above the windshift, the implication is that the cumulus turrets moved with winds at or slightly above the cloud base, and were not representative of the subcloud windfield. It can also be speculated that these clouds were perhaps being sheared from their updrafts, resulting in their limited growth and short lifespans.

3.3 MESOSCALE WAVES

Mesoscale waves were found to exist in the analysis area when tracking was performed on a 1 hour and 15 minute period, movie loop. The computation loop included all available 3-minute SMS pictures from 1939 to 2054 GMT. The vertical motions associated with the mesowaves strongly influenced cloud formation and dissipation over localized areas with their passage. Identifiable elements of the waves were tracked along with cirrus motions, and are presented in Figure 8.

Each wave was characterized by two arced, north-south bands: a cloud (bright) band immediately succeeded by a cloudfree (dark) band. The distance between the cloud and cloudfree bands was about 14 km, giving a measure of the half-wavelength of the mesowave. Since the waves' effects were best exemplified by the transformations of low-level cumuli, it can be estimated from the sounding in Figure 3 that they were centered at a height of about 2.5 km.

The northern portions of each wave exhibited greater arcing and higher velocities than that of the southern portions. Motions of the

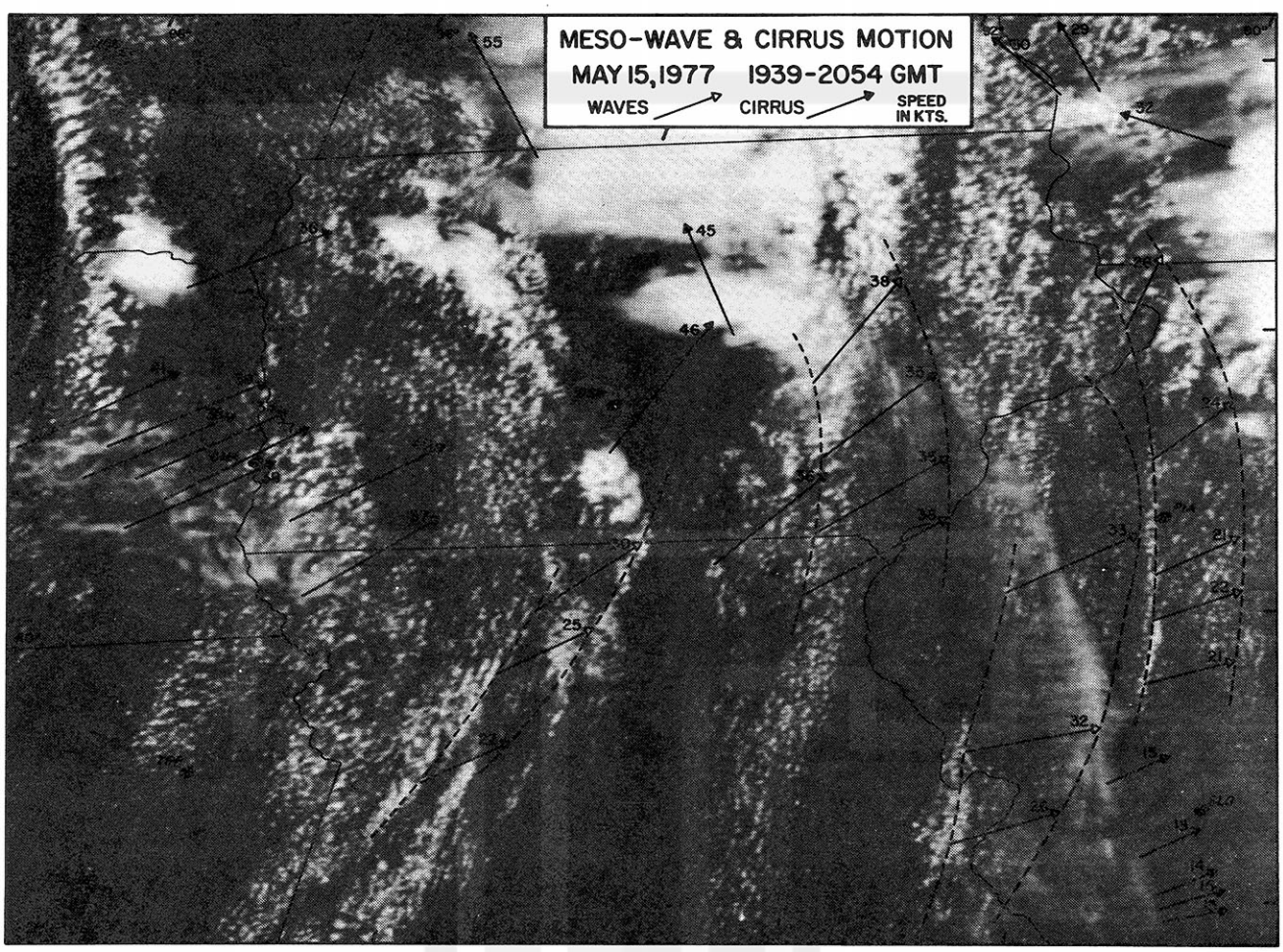

Figure 8. Mesoscale wave and cirrus motions computed from an SMS picture movie loop from 1939 to 2045 GMT, May 15, 1977. Dashed lines show the beginning and end positions of each mesowave.

elements within each wave indicated difluence with wave progression.

Further examination of one mesowave's effect on a thunderstorm is given in the next section.

4. SPLITTING ANVIL AND THUNDERSTORM DECAY

Attention was first focused on the peculiar thunderstorm discussed here, during its actual occurrence. While the Cloud-Truth Experiment Lear Jet was refueling at Des Moines, Iowa, NWS radar indicated what appeared to be a hook echo from a new cell about 20 miles to the southeast.

After an immediate Lear Jet takeoff, the hook-shaped echo proved to be false. In-flight observation, however, did find the storm cell to have an unusual and interesting structure.

A photo taken from the Lear Jet (Figure 9) shows that, rather than being a typically well organized and uniform system, the storm appears to be nothing more than a "towering cumulus gone wild". The cumulus column A is shown to be both twisted and tilted in the vertical. Continuous monitoring during two passes at the rear of the cell revealed that, the upper portion of the column exhibited an anticyclonic rotation in contrast to a somewhat cyclonically rotating lower portion. After the second pass, it became obvious that the storm was rapidly decaying and Lear Jet monitoring was discontinued.

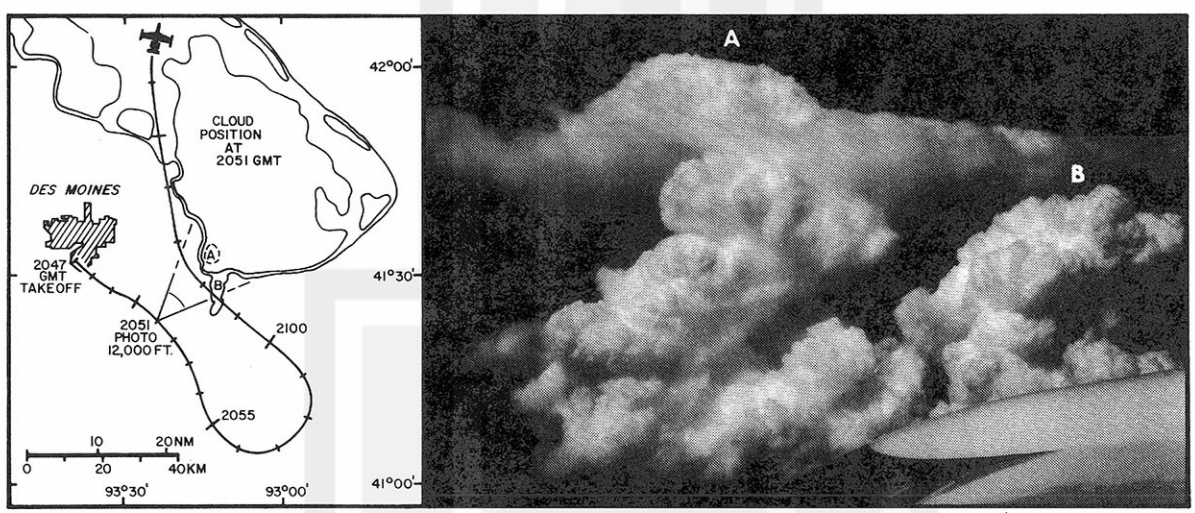

Figure 9. A Lear Jet photo of a thunderstorm which underwent anvil splitting and rapid decay near Des Moines, Iowa. The adjoining diagram shows the flightpath of the Lear Jet in relation to the storm system. The photo was taken from 12,000 feet at 2051 GMT.

A sequence of 12 satellite pictures, selected from 22 pictures taken between 1930 and 2115 GMT, is shown in Figure 10. The sequence depicts the entire life cycle of the storm system in a 1 hour and 45 minute

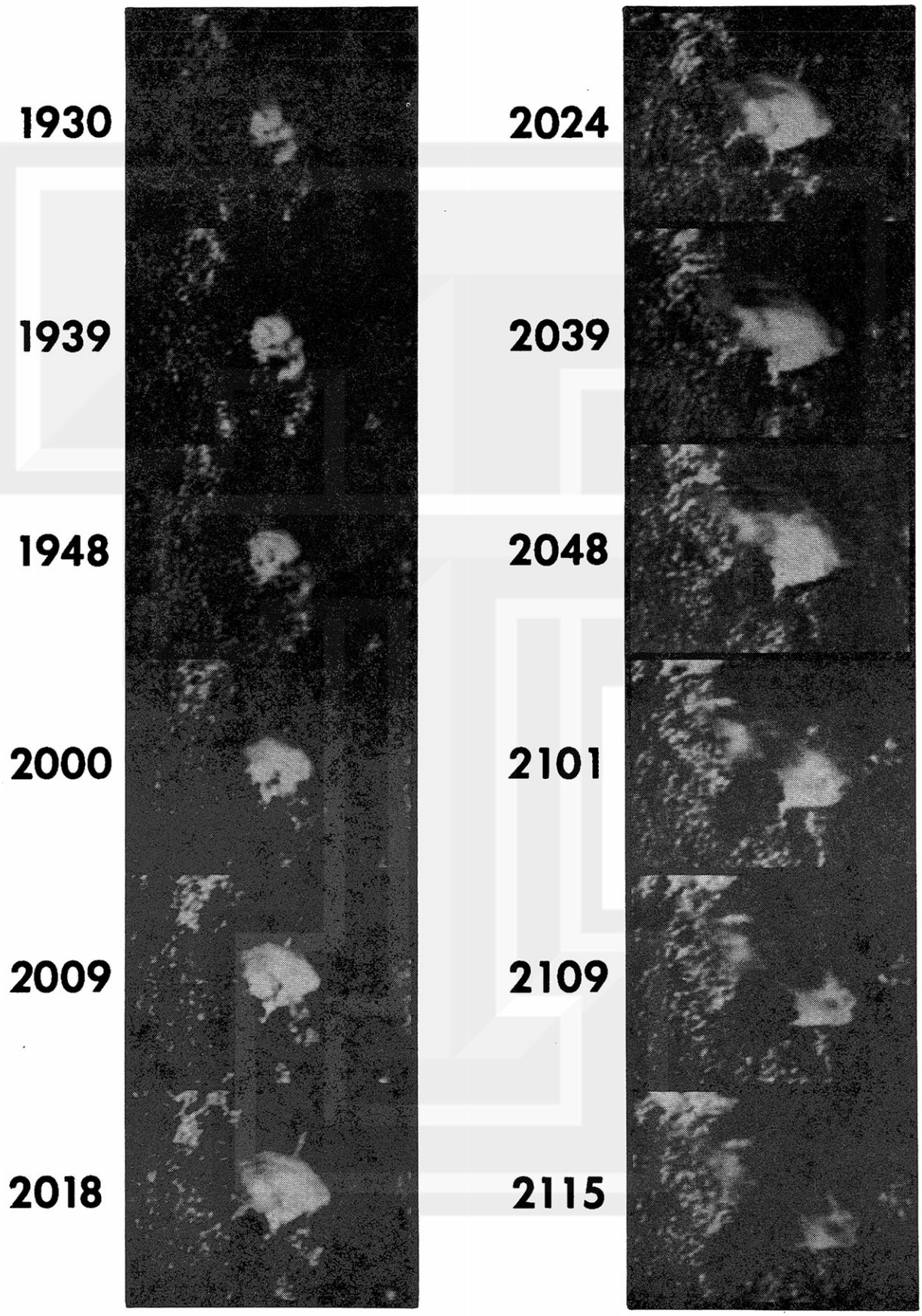

Figure 10. A time sequence of SMS images showing the entire life cycle of a thunderstorm near Des Moines, Iowa. Anvil splitting occurs from 2039 to 2115 GMT. Each picture covers about 100 nm from top to bottom and across.

period. The system began as a small cluster of turrets on the leading edge of a mesowave. The growing anvil was produced by updrafts of at least three cells occurring sequentially; cell **A** in Figure 9 was the last, while cell **B** did not contribute at all. Gravity waves are evident on the leading edge of the anvil; while the clearing area to the rear of the system is indicative of decending motion. The system was eventually overtaken by the same mesowave which gave it birth, resulting in the suppression of its updraft, and its subsequent decay.

Prior to the storm's decay the anvil had undergone a rare split into two separate and distinct segments. In Figure 10, the left side of the anvil is carried to the northwest while the right side travels eastward with the updraft cell. The split may be caused in part by obstacle flow around the cumulus column (see Figures 4 through 7); however the main factor seems to be a horizontal shear.

As a result of being produced by numerous cells of varying strength and duration, the anvil top was distributed through a layer, rather than being at a set level. Shadow measurements along the right edge resulted in an average height of 7.1 km. Alternately, a 2100 GMT I.R. picture indicated the left side to have a cloud top temperature between -32 and -41°C, which was much colder than the right side and equivalent to a height of at least 8 km. The temperature difference could be the effect of a cold dome, but this would not explain the splitting motion. And, an actual shadow of the higher left side is visible on the lower right side in the 2018 and 2024 GMT pictures of Figure 10. Thus the separate anvil segments, having nonequivalent heights and motions, indicate a pronounced horizontal shear associated with the passing wave.

5. SUMMARY

The detailed analyses presented in this paper demonstrate the importance and usefulness of high resolution, 3-minute SMS imagery to mesoscale study.

Cloud heights were obtained using the geometry of the sun, cloud, and shadow relationship. Through this method, clouds were accurately grouped by type and height, providing greater confidence with which to compare their motions to actual winds. The sparcity of the data, however, suggests a need for higher spacial resolution.

The temporal resolution of the 3-minute SMS imagery allowed overland cumulus turrets to be tracked, thereby providing low-level cloud motion fields. A sounding showed these fields, in contrast to subcloud winds, to be more representative of winds at or slightly above the cloud base.

Several mesoscale waves were also identified, tracked and analyzed. Their influence on cloud development and dissipation were closely followed, including the entire life cycle of a wave induced thunderstorm. The storm was shown to have undergone a horizontal shear, resulting in a dramatic split of its anvil.

Without the high spacial and temporal resolution (0.5 mile, 3-minute) of SMS imagery, such short-lived mesoscale phenomena could easily be missed. Even simple qualitative observation, without attempts at quantitative analysis, would be doubtful. Hopefully, future studies incorporating the use of such imagery will reveal further mesoscale features and their mechanisms.

APPENDIX

Determination of Cloud Height
Using the Geometry of the Sun, Cloud and Shadow Relationship

A brief description of a simple method used to determine the cloud heights for the May 15, 1977, 3-minute SMS imagery is given here. Figure 11 schematically illustrates the geometry involved, while Table 3 provides symbol definitions.

Two assumptions are made to complete the geometry, both of which induce some degree of error. One is that the triangle SBI, formed by the cloud tag shadow, subpoint and image respectively, is on a plane perpendicular to $\overline{TB}$. This assumption ignores topographic changes as well as earth curvature, and is made under the consideration that the area involved is small. The second assumption is that $\overline{IT}$ is parallel to a line connecting the earth's center with the satellite. This means that the satellite, like the sun, is taken to be at an infinite distance from the earth. The resulting error is negligible for the sun but more substantial for the satellite. However, the errors induced by these assumptions can be considered small when compared with the inaccuracy of determining the locations of the cloud tag image (I) and the cloud tag shadow (S) on the satellite imagery. The error from this inaccuracy becomes larger as shadows become short. It must be remembered that the final computed height can only be considered an estimation of the actual cloud top height.

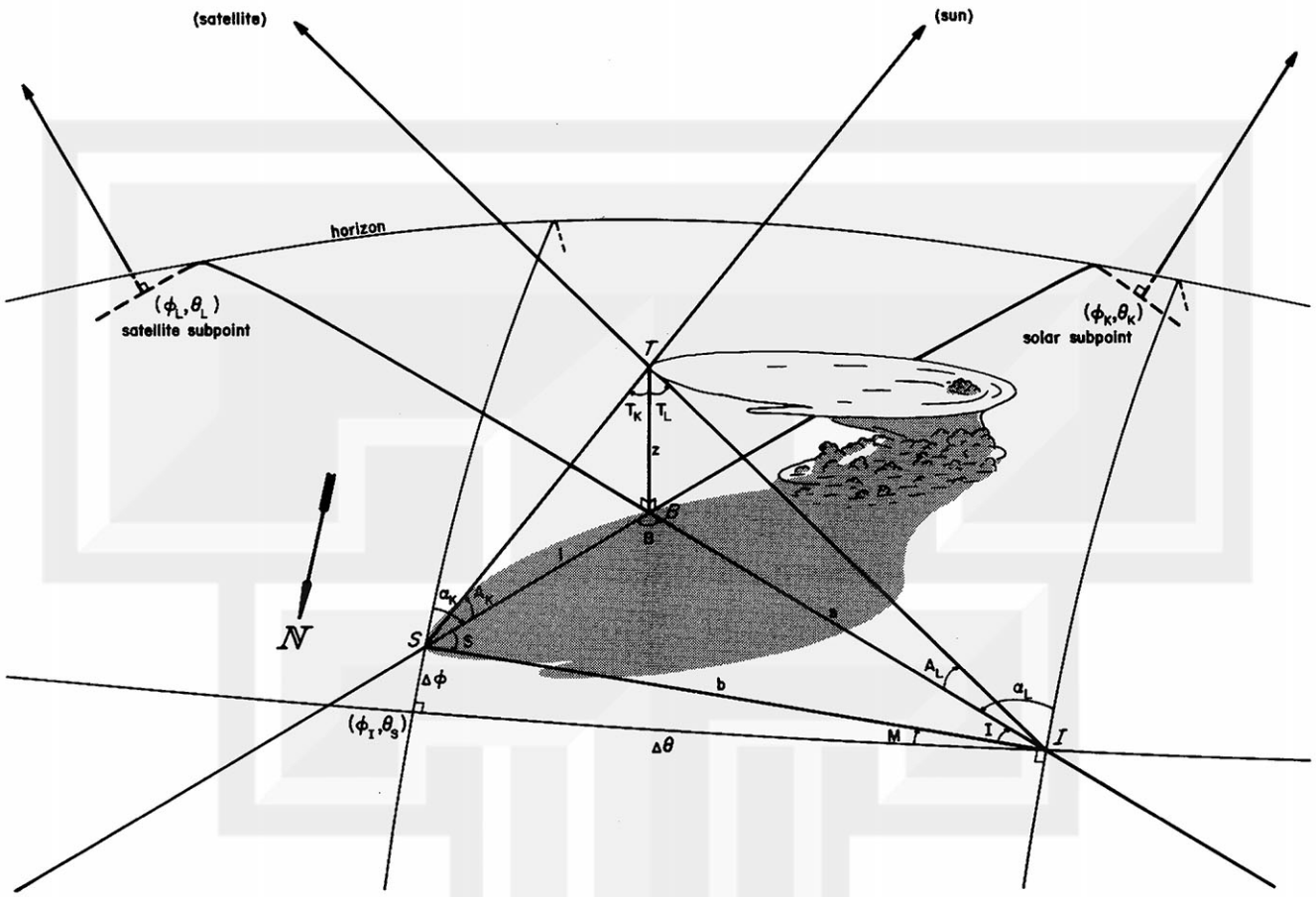

Figure 11. Schematic diagram showing the geometry of the sun, cloud, and shadow relationship used to determine the cloud height (z). Symbol definitions are listed in Table 3.

The known parameters are the solar and satellite subpoints (ϕ_K,θ_K) and (ϕ_L,θ_L) respectively. Points S, (ϕ_S,θ_S) and I, (ϕ_I,θ_I) can be obtained directly from the gridded satellite image. To obtain a measure of $\overline{SI}$ we get

$$\Delta\phi = |\phi_I - \phi_S| \qquad \text{and} \qquad \Delta\theta = |\theta_I - \theta_S| \quad ,$$

which when converted to a non-angular distance will give

$$b = \sqrt{\Delta\phi^2 + \Delta\theta^2} \quad .$$

We also know that

$$M = \arcsin \frac{\Delta\phi}{b} \quad .$$

To obtain values for A_K, A_L, α_K and α_L we use spherical trigonometry, knowing that the solar hour angle $h_K = \theta_K - \theta_S$, and similarly for the satellite, $h_L = \theta_L - \theta_I$. Thus, the solar altitude at S and the satellite altitude at I is

$$A_K = \arcsin(\sin\phi_S \sin\phi_K + \cos\phi_S \cos\phi_K \cos h_K)$$

and

$$A_L = \arcsin(\sin\phi_I \sin\phi_L + \cos\phi_I \cos\phi_L \cos h_L)$$

respectively. Then the azimuth for each is given by

$$\alpha_K = \arcsin \frac{-\cos\phi_K \sin h_K}{\cos A_K}$$

measured from θ_S for the sun, and

$$\alpha_L = \arcsin \frac{-\cos\phi_L \sin h_L}{\cos A_L}$$

measured from θ_I for the satellite.

We can now complete triangle SBI knowing that

$$I = 90 - (\alpha_L + M) \quad \text{and} \quad S = 180 - (B + I) .$$

Therefore

$$i = \frac{b \sin I}{\sin B} \quad \text{and} \quad s = \frac{b \sin S}{\sin B} .$$

Since $T_K = 90 - A_K$ and $T_L = 90 - A_L$, one can complete either of the triangles in the vertical giving the final resulting cloud height above ground level as

$$z = \frac{i \sin A_K}{\sin T_K} = \frac{s \sin A_L}{\sin T_L} .$$

For the case of the May 15, 1977 analysis, a mean elevation of 0.3 km was used for the state of Iowa giving

$$z_{(MSL)} = z_{(AGL)} + 0.3\,\text{km} .$$

Table 3. List of symbols.

T	Cloud tag. The point on the cloud for which the height is to be determined.
I	Cloud tag image. The point on the earth's surface where the cloud tag appears on the satellite image.
S	Cloud tag shadow. The point corresponding to the cloud tag which appears as a shadow on the earth's surface.
B	Cloud tag subpoint.
h	Hour angle.
A	Altitude.
α	Azimuth.
z	Height of the cloud tag above the earth's surface.
ϕ	Latitude.
θ	Longitude.

Subscript K refers to the sun.

Subscript L refers to the satellite.

REFERENCES

Chang, Y. -M., J. J. Tecson and T. T. Fujita, 1973: METRACOM System of Cloud - Velocity Determination from Geostationary Satellite Pictures. SMRP Res. Paper 110, 29 pp.

Forbes, G. S., Personal communication.

Fujita, T. T., E. W. Pearl and W. E. Shenk, 1975: Satellite-tracked cumulus velocities. J. Appl. Meteor., 14, 407 - 413.

_____, 1974: Overshooting thunderheads observed from ATS and Learjet. SMRP Res. Paper 117, 29 pp.

_____, 1970: Basic problems on cloud identification related to the design of SMS - GOES spin scan radiometers. SMRP Res. Paper 84, 33 pp.

Hubert, L. F. and L. F. Whitney, Jr., 1971: Wind estimation from Geostationary Satellite Pictures. Mon. Wea. Rev., 99, 665-672.

Soumi, V. E. et al., 1972: McIDAS, Man - computer Interactive Data Access System. University of Wisconsin - Madison, 39 pp.

Tecson, J. J., T. A. Umenhofer and T. T. Fujita, 1977: Thunderstorm - associated cloud motions as computer from 5-minute SMS pictures. 10th Conf. on Severe Local Storms, Omaha, 22 - 29.

ACKNOWLEDGEMENTS:

The research reported in this paper was sponsored by NASA under grant NGR 14-001-008, and NOAA/NESS under grant NA80AA-D-00001.

Thanks are extended to Dr. T. Theodore Fujita for his continued support and guidance during this project, and Dr. Gregory S. Forbes for his helpful suggestions and assistance.